Lab on a Chip

Cite this: DOI: 10.1039/c1lc20079h

www.rsc.org/loc

PAPER

Direct synthesis and integration of functional nanostructures in microfluidic devices

Jung Kim,[a] Zhiyong Li[b] and Inkyu Park*[a]

Received 30th January 2011, Accepted 22nd March 2011
DOI: 10.1039/c1lc20079h

Integration of functional nanostructures within a microfluidic device can synergize the advantages of both unique properties of nanomaterials and diverse functionalities of microfluidics. In this paper, we report a novel and simple method for the *in situ* synthesis and integration of ZnO nanowires by controlled hydrothermal reaction within microfluidic devices. By modulating synthesis parameters such as the seed preparation, synthesis time, and heating locations, the morphology and location of synthesized nanowires can be easily controlled. The applications of such nanostructure-integrated microfluidics for particle trapping and chemiresistive pH sensing were demonstrated.

Introduction

As the potential applications for personal health care and public security arose, portable and simple assay systems with high performance integrated on a microfluidic platform attracted significant attention over recent years. The advantages of microfluidics include low manufacturing cost, small sample volume per analysis, and increased efficiency and portability.[1] Nanostructures (*e.g.* nanoparticle,[2–4] nanowire,[5–11] nanotube,[12,13] *etc.*) with unique physical and chemical properties are becoming indispensable components of the microfluidic systems. Among them, nanowires have several advantages for microfluidic applications (*e.g.* sensing, filtering, and sample preparation) due to their high surface-to-volume ratio and unique surface properties. A number of groups reported the use of nanowires as materials for bio-sensing[5–8] and chemical-sensing applications.[9–11] Examples include silicon nanowires for protein[5] and virus[6] detection, and ZnO nanowires for pH level[10] and H_2O_2[11] detection. Furthermore, nanowires and nanotubes have been used for the sample preparation and separation in microfluidic devices. G. Chen *et al.* applied nanopillar arrays fabricated by the AAO template method for separation beds or solid-phase reaction in the microchannel.[14] Another example of a nanostructure-integrated microfluidic device is nanopillar arrays fabricated by reactive ion etching (RIE) for DNA separation.[15] Also, in the work of An and Song, a carbon nanotube (CNT) film was used as a DNA separation component within the microchannel.[12] However, for the integration of nanowires or nanotubes within the microfluidic channel, accurate positioning of nanostructures has been a very challenging process. In one method, nanowires or nanotubes were grown using a pre-patterned catalyst, followed by aligned bonding of microfluidic packaging such as PDMS microchannel. For example, CNTs[16] and InP nanowires[17] were fabricated with catalyst patterns by a chemical vapor deposition (CVD) method. However, the CVD method is quite expensive and requires toxic or flammable gaseous materials. Furthermore, the integration of *ex situ* fabricated nanostructures in microchannels with accurate alignment is still a very challenging task. In another method, pre-synthesized nanostructures were assembled by various guiding forces in liquid media. This method can be categorized into two approaches: external guiding force such as dielectrophoretic force,[18] physical fluidic force,[19] surface tension,[20] and magnetic forces;[21] and internal surface interaction such as surface-programmed assembly (SPA)[22] and bio-recognition directed assembly.[23] However, these methods have demonstrated only limited reproducibility, controllability, and yield. Furthermore, mechanical and electrical robustness is not well controlled since the adhesion is made mainly by weak van der Waals force on the surface.

In this work, we report a novel method for *in situ* synthesis and integration of nanowires within the microfluidic device by using hydrothermal reaction. In particular, ZnO nanowires were chosen as the material to be integrated in the microchannel. ZnO nanowires possess many unique properties such as biocompatibility, chemical sensitivity, and piezoelectricity that can be useful for the microfluidic applications.[24] Furthermore, ZnO nanowires can be synthesized by hydrothermal reaction method under 100 °C, which is suitable for the liquid-phase reaction within the microfluidic device.[25] In this article, we demonstrated direct synthesis of ZnO nanowires either on the entire substrate (global synthesis) or at selected locations (local synthesis) on the microfluidic chip. In addition, their applications to particle trapping and pH sensing were demonstrated. We believe this method enables drastically easy and simple *in situ* bottom-up nanowire synthesis within a microfluidic device and can dramatically improve the integration and utilization of nanowires in the microfluidic devices.

[a]*School of Mechanical, Aerospace and Systems Engineering, Division of Mechanical Engineering, KAIST, 291 Daehak-ro, Yuseong-gu, Daejeon, Korea. E-mail: inkyu @kaist.ac.kr; Fax: +82 42 350 3210; Tel: +82 42 350 3233*
[b]*Intelligent Infrastructure Lab, Hewlett Packard Laboratory, 1501 Page Mill Road, Palo Alto, CA, USA*

Experimental

Chemicals and chip fabrication

ZnO nanowires were synthesized by the hydrothermal method suggested by L. E. Greene *et al.*[25] In this work, two types of ZnO seeds were used: texture seeds and e-beam evaporated seeds. 0.005 M zinc acetate dihydrate ($Zn(CH_3COO)_2 \cdot 2H_2O$, 99.0%, JUNSEI) in ethanol were used for texture seeds. The texture seed solution was dropped on the substrate and dried in air for 10 seconds and rinsed with ethanol. The coated substrate was annealed at 350 °C for 20 min. For e-beam evaporated seeds, 10 nm ZnO thin film was deposited on the substrate by e-beam evaporation and annealed at 150 °C for 20 min. For patterned synthesis, photolithography and lift-off process of ZnO thin film seed were employed. Zinc oxide nanowire precursor solution was prepared with zinc nitrate hexahydrate ($Zn(NO_3)_2 \cdot 6H_2O$, 98%, Sigma Aldrich®), hexamethylenetetramine (HMTA, $C_6H_{12}N_4$, 99+%, Sigma Aldrich®) and polyethylenimine (PEI, $(C_2H_5N)_n$, Sigma Aldrich®).[25]

For local synthesis, metal microheaters were fabricated by photolithography and lift-off techniques with Cr (20 nm) and Au (200 nm) layers. Microchannels were fabricated by a conventional PDMS replication technique. Photo-patterned SU-8 structure was used as a master. The channel height was 10 or 20 μm and the widths ranged from 100 μm to 150 μm. The lengths of the channel ranged from 1 cm to 1.5 cm. The fabricated PDMS block with microchannels was bonded to the seeded substrate by a plasma assisted adhesion technique or stamp-and-stick bonding method.[26]

Experiment setup

The schematics of global and local *in situ* ZnO nanowire synthesis and integration in the microfluidic chip are shown in Fig. 1(a) and (b), respectively. For global or patterned synthesis of ZnO nanowires, fresh ZnO nanowire precursor was provided continuously while the temperature of the substrate was maintained at 95 °C by a heating plate. The precursor solution was injected into the microchannel with a flow rate of 1 μL min^{-1} controlled by two syringe pumps (New Era Pump Systems, Inc.), with one at each end of the microchannel. The synthesis time was varied from 1 to 4 hours. For local synthesis by microheater, electrical power was supplied through the microheater while the precursor was flowed through the microchannel. We examined three different electrical power densities to control the morphology and growth rate of the ZnO nanowire arrays.

Preliminary applications

Two preliminary tests were conducted for the application of *in situ* grown nanowires in the microfluidic devices. Firstly, for particle trapping, ZnO nanowire arrays grown from the patterned seed were used as micro-cages to capture silver coated hollow glass microspheres ($d \approx 10$ μm). The spheres were dispersed in ethanol (0.001 g mL^{-1}) and flowed into the microchannel with nanowire arrays at a constant flow rate (0.5 μL min^{-1}). Secondly, to examine the chemical sensing performance, a chemiresistive-type pH sensor was fabricated by making nanowire junctions between two adjacent microheaters to detect pH levels of solutions flowed into the channel. The electrical current through the ZnO nanowire junctions under constant DC bias was measured by using a potentiostat.

Results and discussion

Thermal-fluidic simulation

Fig. 2(a) and (b) show the numerical simulation result of temperature distribution within the microchannel during ZnO nanowire synthesis by using COMSOL Multiphysics™. When the nanowires were synthesized globally, the whole channel was maintained at almost uniform temperature (~95 °C). This suggests that ZnO nanowires can be grown with the uniform

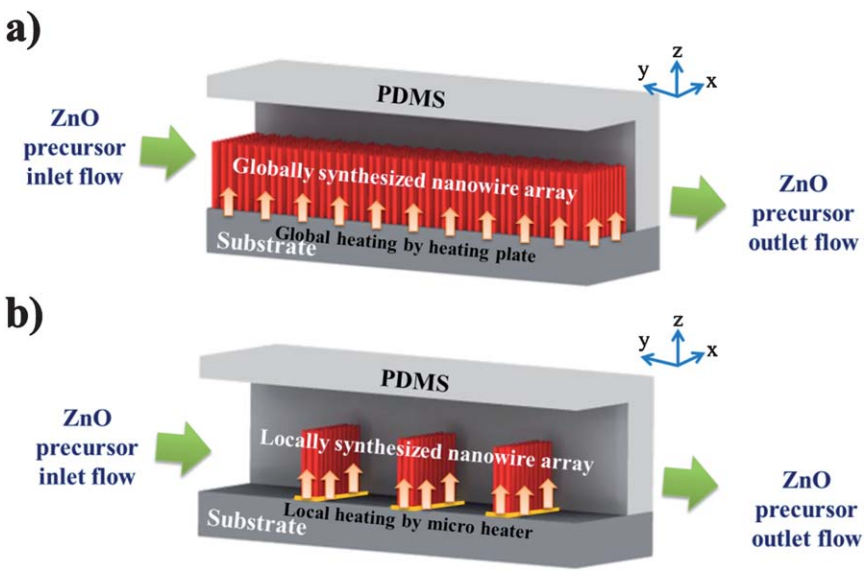

Fig. 1 Schematics of *in situ* synthesis and integration of ZnO nanowires in microfluidic chip: (a) global synthesis in the entire fluidic channel and (b) local synthesis by microheaters in the fluidic channel.

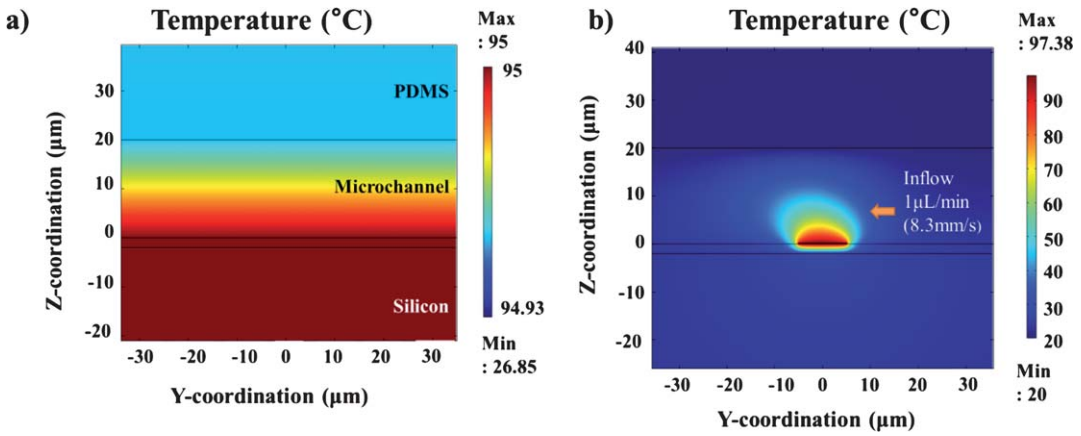

Fig. 2 (a) Numerical simulation of temperature distribution at the center of microchannel during global synthesis process and (b) numerical simulation of temperature distribution near middle microheater during local synthesis process.

growth rate and morphology by heating from the hotplate (Fig. 2(a)). The temperature distribution for the local synthesis process is shown in Fig. 2(b). When the flow rate of the precursor solution is 1 μL min^{-1}, the temperature distribution exhibits asymmetry due to the heat dissipation towards downstream. However, it is observed that the temperature reaches above 90 °C in the vicinity of the microheater, which is sufficient for the ZnO nanowire synthesis. This localized heating enables local synthesis of ZnO nanowires along the microheater.

Global synthesis of ZnO nanowires

After several hours of synthesis, ZnO nanowires were uniformly grown along the microchannel covered by the PDMS block. As shown in Fig. 3(a), ZnO nanowires were uniformly grown within the microchannel after 3 hours except near the sidewall due to the boundary effect. The morphology of the nanowire can be controlled by synthesis time and seed preparation methods.[27] In this work, two kinds of seeds were used for global synthesis: texture and e-beam evaporated seeds. Texture seeds resulted in vertically well-aligned nanowires because the nanowires were grown from the well-established ZnO nanoislands with (0001) plane parallel to the substrate[28] (Fig. 3(b)). In contrast, nanowires grown from e-beam evaporated seeds exhibited a random direction ranging from 45° to 90° with respect to the substrate (Fig. 3(c)). However, the growth rate of the nanowires from e-beam evaporated seeds (~1.3 μm per hour) was faster than those from texture seeds (~0.4 μm per hour). After 4 hours of synthesis, the average lengths of nanowires were 4.8 μm (standard deviation = 280 nm) and 1.4 μm (standard deviation = 260 nm) for e-beam evaporated seeds and texture seeds, respectively. Also, the diameter distribution was narrower by using the e-beam evaporated seeds than by using texture seeds. After 4 hours of synthesis, the average diameters of nanowires were 49 nm (standard deviation = 14 nm) and 88 nm (standard deviation = 38 nm) for e-beam evaporated seeds and texture seeds, respectively. These morphological controls may be utilized for making nanostructures with different shapes for various applications.

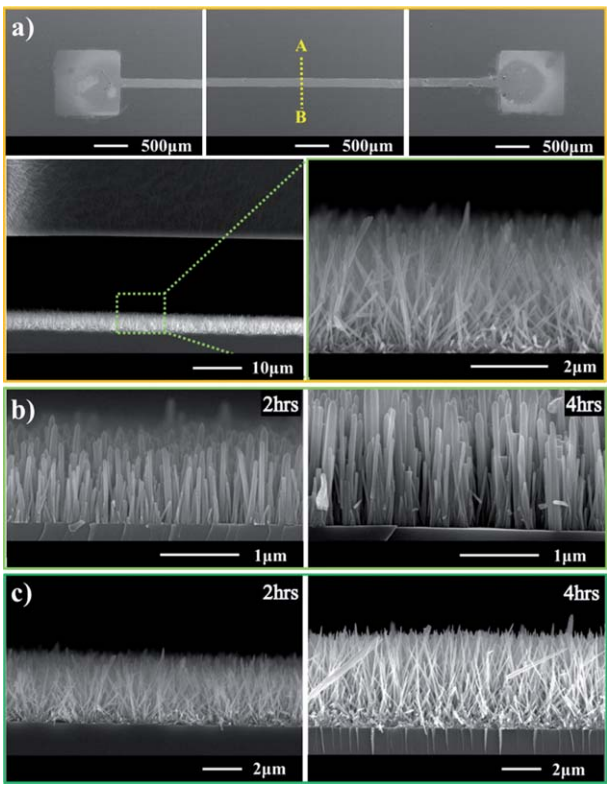

Fig. 3 SEM images of globally synthesized ZnO nanowires with various seeding methods: (a) top and cross-sectional view of ZnO nanowires in microfluidic channels, (b) nanowires grown from texture seed and (c) nanowires grown from e-beam seed.

Patterned synthesis of ZnO nanowire arrays

The patterned synthesis of ZnO nanowire arrays could be realized by using the patterned seeds in the microchannel as shown in Fig. 4. Nanowires were uniformly grown on the dot patterns (15 μm × 15 μm) and line patterns (width: 10 μm and 20 μm). They were also synthesized on various letter patterns ('LabChip', 'KAIST', and 'NANO', width: 20 μm). Very few nanowires could be found outside the original seed patterns. Nanowires from the e-beam evaporated seeds exhibited random directionality, which

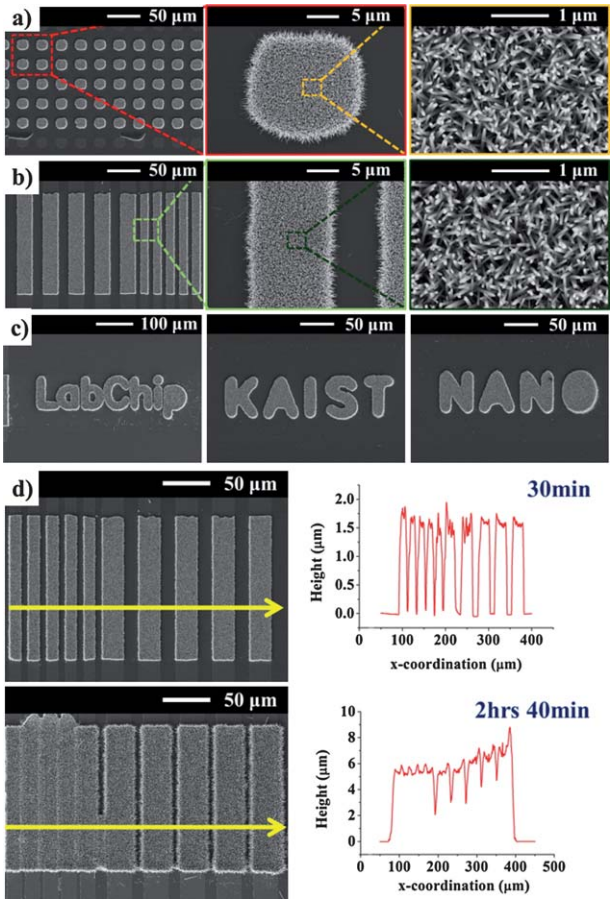

Fig. 4 SEM image of locally synthesized ZnO nanowires from patterned seeding in the microfluidic channel: (a) dot pattern, (b) line pattern and (c) letter patterns ("LabChip", "KAIST" and "NANO") and (d) surface profile of line patterned ZnO nanowire arrays (synthesis time: 30 min and 160 min).

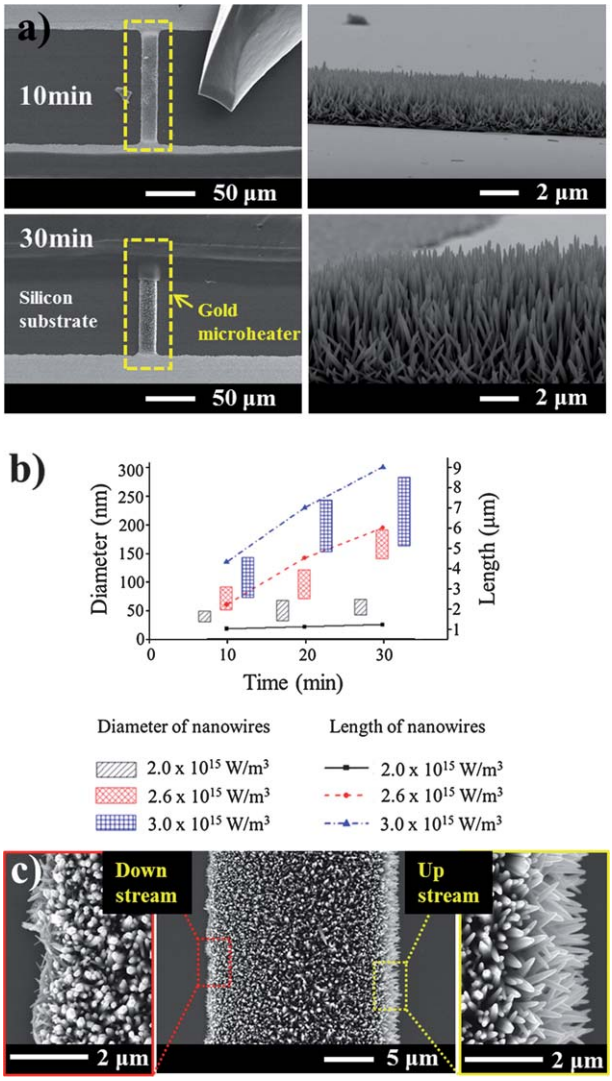

Fig. 5 (a) SEM image of locally synthesized ZnO nanowires by microheater Joule heating: top and cross-sectional views of locally synthesized nanowires grown at power density level of 2.6×10^{15} W m^{-3} and (b) graphs of diameter/length *vs.* time for different power density levels. (c) SEM images of locally grown ZnO nanowires at upstream and downstream edges of the microheater.

resulted in the expansion of the pattern width. Fig. 4(d) shows the profile of the ZnO nanowire arrays measured by a surface profiler (Dektak-8, Veeco). ZnO nanowire arrays grown for 30 min had an average height of 1.5 μm (max. 1.9 μm, min. 1.1 μm) and the widths of nanowire arrays were bigger than the initial seed patterns approximately by +20% due to the dense growth of nanowires. In contrast, the average height of ZnO nanowires grown for 160 min was 6.2 μm (max. 8.8 μm, min. 4.9 μm) and the widths of nanowire arrays were expanded by approximately +100% of the initial seed patterns. A higher and wider nanowire array was synthesized as the synthesis time was extended.

Local synthesis of ZnO nanowire arrays by microheaters

The locally grown ZnO nanowire array by using the microheater is shown in Fig. 5. Nanowires were vertically grown only on the microheater due to the localized endothermic reaction. Here, ZnO nanowire arrays were synthesized at three different electrical power densities (electrical power per volume of the microheater) supplied to the microheaters. As predicted, higher power density caused faster growth rate. The nanowires grown at 2.0×10^{15} W m^{-3} showed relatively nonuniform directionality and very small increase in diameter and length. In contrast, at 3.0×10^{15} W m^{-3}, nanowires grew very fast compared to lower power densities, especially for the first 10 minutes. However, the diameter of nanowires grown at higher power density showed wider distribution than those grown at lower power densities. It is also observed that the nanowires are longer along the upstream edge (right side in Fig. 5(c)) of the microheater than the downstream edge (left side in Fig. 5(c)). This phenomenon might have happened because the upstream side was closer to the inlet port and had a better exposure to the fresh precursor solution while the downstream edge was obstructed from the precursor by the grown nanowires.

Particle trapping

Recently, the importance of single cell study is becoming more emphasized. The conventional bioassay of a large number of cells

provides only average values of cellular behaviors. However, if the deviation of each individual cell is significant, single cell study is essential for better understanding of the cellular behavior. For this purpose, single cell separation and trapping in the microfluidic systems have been actively explored.[29–31] Previous studies have used cell trap sites based on PDMS[28,29] or silicon[30] walls for single cell trapping. We expect that ZnO nanowires grown in the microfluidic channel can also function as structures for single cell trapping. The patterned nanowire array allows the trapping of cells whose diameters are much bigger than the gap between nanowires. Meanwhile, the porous nature of the nanowire array minimizes the blockage of the flow. This allows effective trapping of cells with minimal obstruction to the sample flow and concomitant physical stress to the cells.

As a preliminary step for this potential application, we have demonstrated the trapping of microparticles by micro-cages based on patterned ZnO nanowire arrays. As shown in Fig. 6(a), silver coated hollow glass microspheres were captured in the U-shaped micro-cages while the dispersion media (ethanol) flew out through the porous network of nanowires. When the particles encountered the nanowire bundle-based cages along the flow streamline, they could escape from the cages due to the geometric confinement by the cages. The captured microspheres maintained to be captured in the nanowire-based micro-cages, and this suggests their potential as single cell trapping structures.

pH sensing

The pH sensitivity of electrical conductance through ZnO nanowires allows their application to pH sensing. Since ZnO nanowire is an n-type semiconductor, it changes its surface electron charge by the surrounding ion charge concentration. This change of surface charge causes electrical conductance modulation at different pH levels.[32] The conductance of the nanowires decreases as the pH level is increased due to the formation of a depletion layer at the surface. To demonstrate a ZnO nanowire-based pH sensor, a nanojunction of ZnO nanowire arrays was fabricated by using two adjacent microheaters as shown in Fig. 6(b). The electrical characterization and pH sensing result are shown in Fig. 6 (c). In DI water environment, the *I–V* characteristics show a Schottky contact-type behavior with low electrical conductance (~0.1 mS at 1 V). By changing the liquid from DI water to pH = 7 buffer solution, more Ohmic behavior was observed with an enhanced electrical conductance (~0.4 mS at 1 V). This can be attributed to the dissolved ions in the pH buffer solution playing a role in the electrical current between the synthesized nanowires. Next, a real-time pH sensing was conducted with a constant DC bias of 0.2 V across the nanowire junction. The current through the ZnO nanowire junction decreased as the pH level was increased. The current was significantly dropped from 26.6 μA to 20.7 μA when the pH level was switched from pH = 5 to pH = 6. However, the current change became smaller at higher pH levels (*e.g.* $I = 19.2\ \mu A \rightarrow 18.8\ \mu A$ for pH = 8 → 9). Although the sensor response was not linear with respect to the pH level change, the general trend of decreasing the conductance by increasing the pH level for n-type semiconducting ZnO nanowires was consistent with our theoretical expectation. Also, the sensor exhibited a reasonable sensitivity to the pH levels from pH = 5 to pH = 9. The nonlinearity may be caused by the nonlinear dependence of the surface charge on the pH level of the solution and density limit of available binding sites for H^+ and OH^- ions. For better performance, the morphology and surface control of the nanowire junction and sensing parameters such as operation voltage and frequency should be optimized.

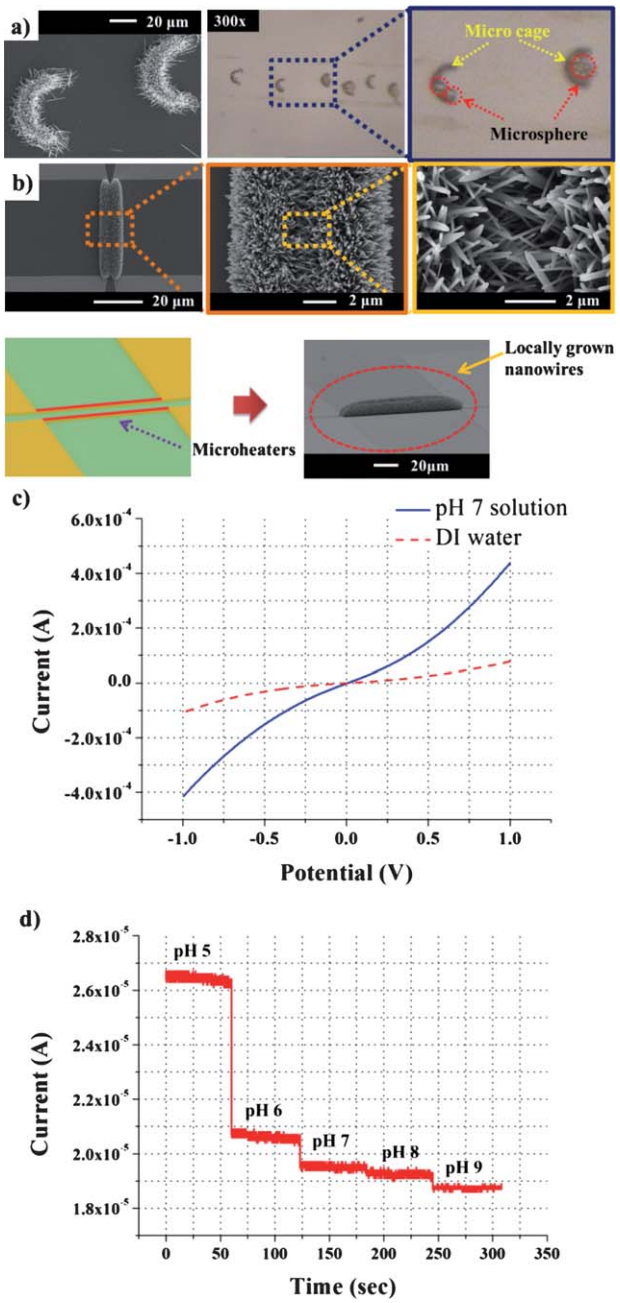

Fig. 6 Applications of *in situ* synthesized ZnO nanowires: (a) particle trapping by micro-cage based on locally grown nanowires, (b) SEM images of ZnO nanowire bridging grown by microheater Joule heating, (c) current–voltage (*I–V*) characterization of ZnO nanowire bridge in DI water and pH 7 solution and (d) pH sensing by ZnO nanowire bridge.

Conclusion

Here we have introduced a novel method for *in situ* nanowire synthesis and direct integration within the microfluidic device *via*

the hydrothermal synthesis method. By this simple method, ZnO nanowires could be synthesized either on the entire substrate, patterned area, or along the microheaters within the microfluidic device. This novel method has several advantages for the realization of nanostructure-integrated microfluidic devices: (1) eco-friendly process with benign chemistry and low-temperature conditions, (2) facile and direct integration of nanostructures in the microfluidic chip without complicated and inaccurate alignment and integration procedures required, and (3) controlled and facile localization of nanostructures within the microchannel for diverse applications. We have also demonstrated the potential of ZnO nanowire arrays fabricated by this method for applications to particle trapping and pH level sensing. Based on these results, we conclude that the proposed method can be applied to various microfluidic applications such as biochemical sensing and single cell studies with improved device performances by using unique characteristics of functional nanostructures.

Acknowledgements

This research was supported by Basic Science Research Program (2010-0015290) and Future-based Technology Development Program (Nano Fields) (2009-0082529) through the National Research Foundation of Korea (NRF) funded by the Ministry of Education, Science and Technology and Open Innovation Research Program of Hewlett Packard (HP) Company.

References

1 C. M. Leiber, *MRS Bull.*, 2003, **28**, 486–491.
2 K. S. Kim and J.-K. Park, *Lab Chip*, 2005, **5**, 657–664.
3 C. Huang, K. Bonroy, G. Reekmans, W. Laureyn, K. Verhaegen, I. D. Vlaminck, L. Lagae and G. Borghs, *Biomed. Microdevices*, 2009, **11**, 893–901.
4 J. J. Lai, J. M. Hoffman, M. Ebara, A. S. Hoffman, C. Estournès, A. Wattiaux and P. S. Stayton, *Langmuir*, 2007, **23**, 7385–7391.
5 Y. Cui, Q. Wei, H. Park and C. M. Lieber, *Science*, 2001, **293**, 1289–1292.
6 F. Patolsky, G. Zheng, O. Hayden, M. Lakadamyali, X. Zhuang and C. M. Leiber, *Proc. Natl. Acad. Sci. U. S. A.*, 2004, **101**, 14017–14022.
7 K. Yang, G.-W. She, H. Wang, X.-M. Qu, X.-H. Zhang, C.-S. Lee and S.-T. Lee, *J. Phys. Chem. C*, 2009, **113**, 20169–20172.
8 A. Umar, M. M. Rahman, A. Al-Hajry and Y.-B. Hahn, *Talanta*, 2009, **78**, 284–289.
9 I. Park, Z. Li, A. P. Pisano and R. S. Williams, *Nanotechnology*, 2010, **21**, 105501.
10 S. J. Pearton, W. T. Lim, J. S. Wright, L. C. Tien, H. S. Kim, D. P. Norton, H. T. Wang, B. S. Kang, F. Ren, J. Jun, J. Lin and A. Osinsky, *J. Electron. Mater.*, 2008, **37**, 1426–1432.
11 J. Liu, C. Guo, C. M. Li, Y. Li, Q. Chi, X. Huang, L. Liao and T. Yu, *Electrochem. Commun.*, 2009, **11**, 202–205.
12 Y.-H. An and S. Song, *Mol. Cell. Toxicol.*, 2006, **2**, 279–284.
13 Q. Fu and J. Liu, *J. Phys. Chem. B*, 2005, **109**, 13406–13408.
14 G. Chen, G. T. McCandless, R. L. McCarley and S. A. Soper, *Lab Chip*, 2007, **7**, 1424–1427.
15 J. Shi, A. P. Fang, L. Malaquin, A. Pépin, D. Decanini, J. L. Viovy and Y. Chen, *Appl. Phys. Lett.*, 2007, **91**, 153114.
16 S. J. Kang, C. Kocabas, T. Ozel, M. Shim, N. Pimparkar, M. A. Alam, S. V. Rotkin and J. A. Rogers, *Nat. Nanotechnol.*, 2007, **2**, 230–236.
17 T. Mårtensson, M. Borgström, W. Seifert, B. J. Ohlsson and L. Samuelson, *Nanotechnology*, 2003, **14**, 1255–1258.
18 R. Krupke, F. Hennrich, H. v. Löhneysen and M. M. Kappes, *Science*, 2003, **301**, 344–347.
19 Y. Huang, X. Duan, Q. Wei and C. M. Leiber, *Science*, 2001, **291**, 630–633.
20 D. Whang, S. Jin, Y. Wu and C. M. Leiber, *Nano Lett.*, 2003, **3**, 1255–1259.
21 C. M. Hangarter, Y. Rheem, B. Yoo, E.-H. Yang and N. V. Myung, *Nanotechnology*, 2007, **18**, 205305.
22 S. G. Rao, L. Huang, W. Setyawan and S. Hong, *Nature*, 2003, **425**, 36–37.
23 A. K. Salem, J. Chao, K. W. Leong and P. C. Searson, *Adv. Mater.*, 2004, **16**, 268–271.
24 Z. L. Wang, *Mater. Sci. Eng., R*, 2009, **64**, 33–71.
25 L. E. Greene, B. D. Yuhas, M. Law, D. Zitoun and P. Yang, *Inorg. Chem.*, 2006, **45**, 7535–7543.
26 S. Satyanarayana, R. N. Karnik and A. Majumdar, *J. Microelectromech. Syst.*, 2005, **14**, 392–399.
27 M. Guo, P. Diao and S. Cai, *J. Solid State Chem.*, 2005, **178**, 1864–1873.
28 L. E. Greene, M. Law, D. H. Tan, M. Montano, J. Goldberger, G. Somorjai and P. Yang, *Nano Lett.*, 2005, **5**, 1231–1236.
29 D. D. Carlo, L. Y. Wu and L. P. Lee, *Lab Chip*, 2006, **6**, 1445–1449.
30 D. D. Carlo, N. Aghdam and L. P. Lee, *Anal. Chem.*, 2006, **78**, 4925–4930.
31 A. Valero, F. Merino, F. Wolbers, R. Luttge, I. Vermes, H. Andersson and A. v. d. Berg, *Lab Chip*, 2005, **5**, 49–55.
32 A. Fulati, S. M. U. Ali, M. Riaz, G. Amin, O. Nur and M. Willander, *Sensors*, 2009, **9**, 8911–8923.

